Microarticle

Modified solvothermal synthesis of cobalt ferrite (CoFe$_2$O$_4$) magnetic nanoparticles photocatalysts for degradation of methylene blue with H$_2$O$_2$/visible light

Abul Kalam [a,b,*], Abdullah G. Al-Sehemi [a,b], Mohammed Assiri [a,b], Gaohui Du [c], Tokeer Ahmad [d], Irfan Ahmad [a,b], M. Pannipara [a,b]

[a] Department of Chemistry, Faculty of Science, King Khalid University, Abha 61413, P.O. Box 9004, Saudi Arabia
[b] Research Center for Advanced Materials Science (RCAMS), King Khalid University, Abha 61413, P.O. Box 9004, Saudi Arabia
[c] Zhejiang Key Laboratory for Reactive Chemistry on Solid Surfaces, Institute of Physical Chemistry, Zhejiang Normal University, Jinhua 321004, China
[d] Nanochemistry Laboratory, Department of Chemistry, Jamia Millia Islamia, New Delhi 110025, India

ARTICLE INFO

ABSTRACT

Different grads of magnetic nano-scaled cobalt ferrites (CoFe$_2$O$_4$) photocatalysts were synthesized by modified Solvothermal (MST) process with and without polysaccharide. The indigenously synthesized photocatalysts were characterized by means of X-ray diffraction (XRD), scanning electron microscopy (SEM), transmission electron microscopy (TEM), high-resolution transmission electron microscopy (HRTEM), thermo gravimetric analysis (TGA), Fourier transform infrared (FT-IR), UV–visible (UV–vis) spectroscopy and N$_2$ adsorption–desorption isotherm method. The Fourier transform infrared spectroscopy study showed the Fe-O stretching vibration 590–619 cm^{-1}, confirming the formation of metal oxide. The crystallite size of the synthesized photocatalysts was found in the range between 20.0 and 30.0 nm. The surface area of obtained magnetic nanoparticles is found to be reasonably high in the range of 63.0–76.0 m^2/g. The results shown that only MST-2 is the most active catalyst for photo-Fenton like scheme for fast photodegradation action of methylene blue dye, this is possible due to optical band gap estimated of 2.65 eV. Captivating the percentage of degradation efficiency increases up to 80% after 140 min by using MST-2 photocatalyst. Photocatalytic degradation of methylene blue (MB) dye under visible light irradiation with cobalt ferrite magnetic nanoparticles followed first order kinetic constant and rate constant of MST-2 is almost 2.0 times greater than MST-1 photocatalyst.

Introduction

Globally, approximately 10,000 types of dyes and pigments are manufactured by the year. In textile industries, about 20–30% natural and synthetic dyes are wasted in industrial sewages during processing. Most of them are very toxic due to the presence of non-biodegradable aromatic structure, which affects negative influences on human health, microorganisms and ecological safety. Thus, conventional treatments like ion exchange, precipitation, coagulation and flocculation, membrane filtration, electrochemical and biological methods have been proposed [1,2].

To overwhelm the disadvantages of conventional treatments, advanced oxidation processes (AOP) are performed as an emerging devastation technology for degradation of organic pollutants in waste water [3–5]. Therefore, the photo-Fenton treatment is a proficient and inexpensive technique for treatment of waste water [6–9]. This type of treatment is ascribed to their production of highly reactive, powerful oxidant and non-selective reagent hydroxyl radicals (OH·) due to the catalytic decomposition of hydrogen peroxide (H$_2$O$_2$) by the iron ions [1,5,8]. Due to high oxidation potential of hydroxyl radical (2.80 V) favors the destruction and decomposition of non-biodegradable organic pollutants, unsaturated compounds in aqueous solution and finally produces carbon dioxide, water and other substances [1,2,4,10,11].

Recently, there is an enormous challenge for the world material scientists to design new materials with enhanced physico-chemical properties and different synthetic methods to accomplish world technological demand. Spinel ferrite (MFe$_2$O$_4$) magnetic nanocomposites have fascinated much responsiveness owing to their distinctive magnetic assets and chemical stability [12–13].

* Corresponding author.
   E-mail address: abulkalam@kku.edu.sa (A. Kalam).

It can be very easy to remove spinel ferrites magnetic nanocomposites from the treated waste by applying external magnetic material and recycled [14–16]. Cobalt ferrite (CoFe$_2$O$_4$) magnetic nanocomposites are indispensable metal oxide as compared to other spinel ferrites because they have exclusive applications in various fields like sensor [17,18], semiconductor photocatalysts [19,20], biomedical [21], cancer treatment [22], magnetic optical behavior [23], electrical [24] and antibacterial [25]. It is n-type semiconductor, highly stable, small optical band gaps (2.0 eV) making them active under visible light treatment [26,13]. For these purposes, the syntheses of cobalt ferrite magnetic nanocomposite with control morphology to tune their physical and chemical properties are quite imperative.

Therefore, several techniques such as hydrothermal [27], co-precipitation [28], ball milling [29], micro-emulsion [30], sol-gel [31] and electrospining [32] are used for the synthesis of cobalt ferrite nanocomposites. Among them only modified solvothermal method is designed to achieve targeted results such as virtuous homogeneity, controlled crystallite size, high limpidness and low agglomeration.

To achieve this, we were synthesized cobalt ferrite magnetic nanoparticles through modified solvothermal method and characterized by using X-ray diffraction (XRD), scanning electron microscopy (SEM), transmission electron microscopy (TEM), high-resolution transmission electron microscopy (HRTEM), thermo gravimetric analysis (TGA), Fourier transform infrared (FT-IR), UV–visible (UV–vis) spectroscopy and Brunauer-Emmett-Teller (BET) method. Along with this, we performed the photocatalytic activity of cobalt ferrite magnetic nanoparticles for degradation of MB with H$_2$O$_2$ under visible light irradiation.

Experimental

Materials

The chemicals which were used in this experiment including cobalt chloride [Sigma-Aldrich, USA], ferric chloride [Sigma-Aldrich, USA], sodium hydroxide [Sigma-Aldrich, USA], H$_2$O$_2$ (PRS Panreac), starch (Sigma-Aldrich, USA), cellulose (Sigma-Aldrich, USA) and methylene blue [Sigma-Aldrich, USA] were of analytical grade and used as received.

Synthetic procedure

The Cobalt ferrite magnetic nanoparticles were synthesized by modified solvothermal method using stoichiometric amount of 0.6 M ferric chloride hexahydrate (FeCl$_3$·6H$_2$O) and 0.3 M cobalt chloride hexahydrate (CoCl$_2$·6H$_2$O) dissolved in the double distilled water. Then 3 M NaOH solutions were added drop-wise into the above solution to increase the pH of the solution. After 30 min, ethanol was also added to the system to form the low boiling azeotrope mixture with water.

The whole mixture was further stirred on magnetic stirrer for 12 h at 80 °C to obtain the precipitate. After completing the reaction, precipitates were collected by centrifugation at 5000 rpm and washed with double distilled water and acetone several times until pH was obtained. The precipitates were then dried overnight in an oven at 100 °C and abbreviated by MST-1.

Similarly, we obtained second and third samples (MST-2 and MST-3) by same procedure but in which 2.0 g cellulose and starch was added and the mixture was stirred for 1 h. Then 3 M NaOH was added drop-wise into the above solution to increase the pH of the solution, respectively. The as-synthesized powders were calcined at 400 °C for 2 h in muffle furnace to get CoFe$_2$O$_4$ magnetic nanoparticles.

Instrumental techniques

The calcined cobalt ferrite magnetic nanoparticles were characterized by X-ray diffractometer (XRD) (Philips PW3040/60) fitted out with Cu-Kα radiation (λ = 1.5418 Å). Diffractograms of the prepared samples were noted at room temperature using an angular range of 2θ = 10°–70° at an increment of 0.02° and scan rate of 2° min^{-1}. The scanning electron microscopy (SEM; Hitachi S4800) was used to study the surface morphologies of cobalt ferrite magnetic nanoparticles. The JEOL 2100F transmission electron microscopy (TEM) and high resolution transmission electron microscopy (HR-TEM) were used to examine the grain size and morphology of cobalt ferrite magnetic nanoparticles working at 200 kV. The TEM samples were prepared by the ultrasonic dispersion of small amount of the powders in a few milliliters of ethanol, and then dropping on a copper grid covered in an amorphous carbon film. The Specific surface area, total pore volume and pore size distribution of the powder samples were measured on B.E.T. surface area analyzer (Model 2000e, Quantachrome USA). Samples were primarily evacuated and degassed at 200 °C for 2 h before the analysis. The surface area of cobalt ferrite magnetic nanoparticles was determined by the multi-point Brunauer–Emmett–Teller (BET) method, pores size and pore volume was determined by using Barrett–Joyner–Halanda (BJH) method, DH and DA method. Ultra violet-visible absorption (UV–vis) spectra of the samples were recorded using PG UV–vis double-beam spectrophotometer in the wavelength range of 250–800 nm. Infrared absorption spectroscopy (IR) spectra were recorded at room temperature on a FTIR spectrometer (JASCO 460 plus) using the KBr pellet technique. The thermal behavior was investigated using TGA analysis (Shimadzu TGA 50). For TG a ceramic sample boat was used with the sample size being 10.0 ± 0.1 mg. Curves were recorded upon heating from room temperature up to 800 °C at 10 °C/min and 30 ml/min flow of nitrogen atmosphere. The solar light simulator (USA) was used for the degradation of methylene blue dye.

Photocatalytic degradation of MB

The photocatalytic recital of cobalt ferrite magnetic nanoparticles was assessed by degradation of MB solution under a solar simulator. The 50 ml of MB solution (10 ppm) was mixed with 0.01 g/l of catalyst in a 250 ml beaker and the mixture was stirred in dark place for 30 min to get equilibrium. Later, the whole mixture was place under solar simulator and irradiated to induce the photo-
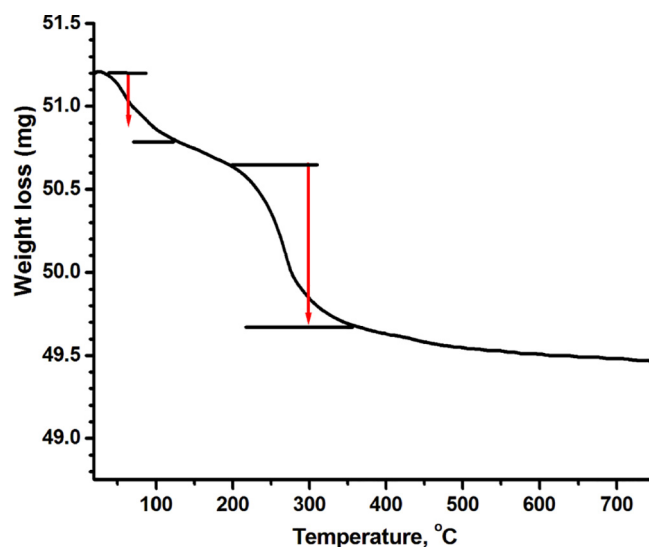

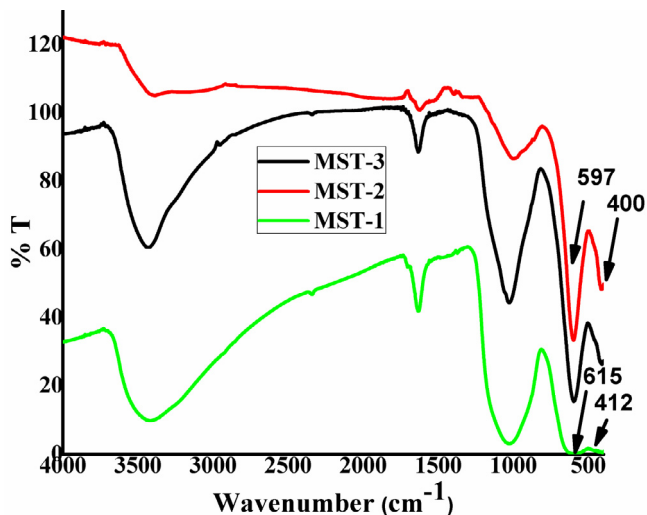**Fig. 1.** TGA of the modified Solvothermal synthesized sample (MST-3).

Fig. 2. FTIR of the modified Solvothermal synthesized samples (MST-1, MST-2 and MST-3).
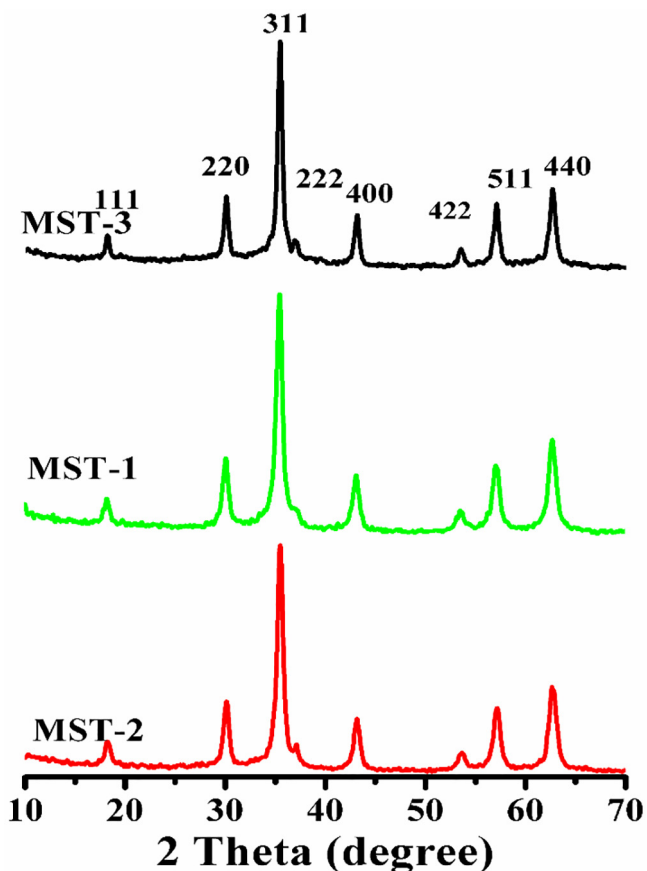

Fig. 3. X-ray diffraction patterns of the modified Solvothermal synthesized samples (MST-1, MST-2 and MST-3).

chemical reaction. The photodegradation of MB was enhanced by the addition of 5.0 mM H_2O_2 generating heterogeneous photo-Fenton system. The photodegradation process was monitored by the absorbance and measured by using a UV–vis spectrophotometer (PG instrument) for each sample.

Results and discussion

Thermo gravimetric analysis was castoff to study the thermal stability of the synthesized cobalt ferrite magnetic nanoparticles samples which is based on weight loss as a function of temperature. Fig. 1 shows the TGA curves recorded for the sample MST-3 heated up to 800 °C at 10 °C/min in the air atmosphere. The TGA curves indicate that the sample MST-3 decomposes in two steps. The first weight loss occurs between 50 and 125 °C, corresponding to the evaporation of physically adsorbed water on the surface of cobalt ferrite material. The second weight loss occurs in the temperature range 200–350 °C, which may be ascribed to the removal of NaOH, chloride and coordinated water adsorbed at the surface of metal hydroxide and finally to the decomposition of the hydroxide and pyrolysis of the starch moieties with maximum weight loss. When temperature was higher than 350 °C, almost all starch was pyrolyzed. The weight loss of the steps is about 3.483% and 8.33%. Based on the results of TGA, the temperature of 400 °C was chosen to ensure the complete decomposition of precursor to form $CoFe_2O_4$. After the calcination at 400 °C for 2 h in air, the FTIR and XRD pattern resulted in all the peaks corresponding to $CoFe_2O_4$ with a face centered cubic structure.

Structural properties

The FTIR spectra of calcined cobalt ferrite magnetic nanoparticles are shown in Fig. 2. It is an ideal technique to identify the chemical structural changes occurring in the materials and the positions occupied by the ions. The calcined cobalt ferrite magnetic nanoparticles exhibit two main vibration bands at 597–615 (υ_1) and at 412–400 (υ_2) cm^{-1} corresponding to the stretching vibration of M−O bond in tetrahedral and octahedral sites. According to Raut et al. [33] vibration mode between tetrahedral metal ion and oxygen complex gives rise to high frequency band in the range of 590–619 cm^{-1} while, stretching vibration between octahedral metal ion and oxygen complex gives rise to weak frequency band in the range of 420–450 cm^{-1} in case of inverse spinel ferrites. The vibration frequency depends on cation mass, cation- oxygen distance and the bonding force for tetrahedral and octahedral complexes. In the present study, the υ_1 frequency for the MST-1 sample was 615.80 and it was 597.30 and 597.30 for samples MST-2 & 3. From Fig. 2, it is obvious that, by polysaccharides (MST-2 and MST-3), the υ_1 and υ_2 band shifted towards lower frequency. This change in υ_1 and υ_2 band may be attributed to the changes in bond length of oxygen (O^{2-}) and metal ions (Co^{2+} and Fe^{3+}) at tetrahedral and octahedral sites [33]. The FTIR results confirmed that the samples have spinel structure of $CoFe_2O_4$, which were revealed by the XRD results.

Fig. 3 revealed the X-ray diffraction patterns of the samples (MST-1, MST-2 and MST-3) and results displays sharp and strong

Table 1
Data of crystallite size, inter-planer spacing, lattice constant, particle size and band gap energy of $CoFe_2O_4$ samples.

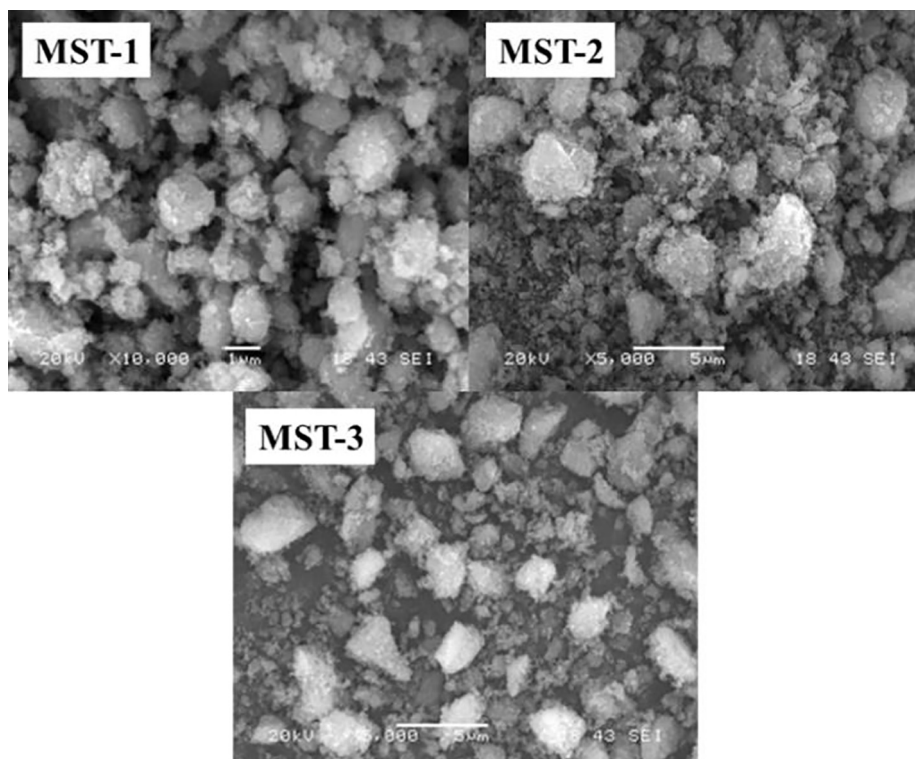| Sample	Position of 311 peak (degree)	Crystallite size (XRD; nm)	Interplaner spacing (d$_{311}$; nm)	Lattice constant (a; nm)	Average Particle Size (TEM; nm)	Optical Band Gap (Eg; eV)
MST-1	35.484	15.0	0.2529	0.838	30.0	2.5
MST-2	35.469	11.85	0.2533	0.840	20.0	2.65
MST-3	35.435	12.38	0.2530	0.839	22.0	2.6

Fig. 4. SEM images of the samples (MST-1, MST-2 and MST-3) nanoparticles.
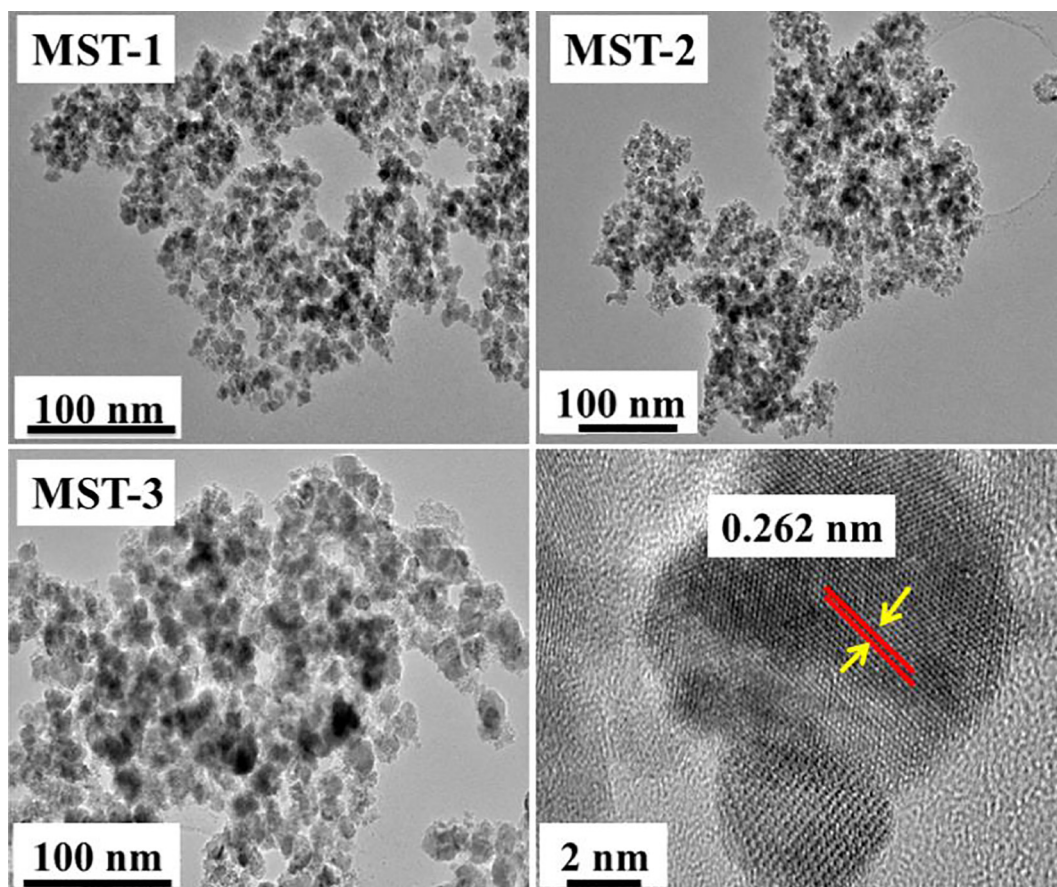

Fig. 5. TEM images of the samples (MST-1, MST-2 and MST-3) nanoparticles and HRTEM image showing the (3 1 1) planes.

reflections which could be indexed on the basis of pure spinel cobalt ferrite magnetic nanoparticles having face centered cubic structure. The planes with h k l values of (1 1 1), (2 2 0), (3 1 1), (2 2 2), (4 0 0), (4 2 2), (5 1 1) and (4 4 0) could be matched correctly with the standard X-ray diffraction pattern of monophasic spinel cobalt ferrite magnetic nanoparticles (space group Fd-3m, JCPDS card No. 22-1086) [34]. The broadening of X-ray diffraction peak represents the nanocrystalline nature of the spinel cobalt ferrite magnetic nanoparticles. The crystallite size (d) of spinel cobalt ferrite magnetic nanoparticles were calculated from the most intense peak (3 1 1) by using the Debye–Scherrer formula [35,36], as shown in Table 1.

$$d = 0.9\lambda/\beta\cos\theta$$

where λ is the wavelength of X-ray (Cu Kα = 0.154 nm), d is the size of crystallite (nm), β is the full width at half maximum (FWHM) of prominent intense peak measured in radians, and θ is peak angle [37,38]. Table 1 shows the crystallite size of synthesized materials determined by using the X-ray line broadening studies and the results are close to the values obtained from TEM analysis. The lattice constant (a) of spinel cobalt ferrite magnetic nanoparticles were calculated by using the most intense peak (3 1 1) and by using the equation [39]:

$$a = d_{hkl}\sqrt{h^2 + k^2 + l^2}$$

where d is interplanar distance, a is lattice constant and h k l are Miller indices. The observed inter-planar d-spacing and lattice constant for all synthesized nanoparticles are also shown in Table 1. The results showed that the lattice constant of sample MST-2 increases and crystallite size decreases. This might be due to influence and scratch forces created inside and further smashed into smaller nano scale.

Morphological properties

Fig. 4 displays the images of cobalt ferrite magnetic nanoparticles using Scanning electron microscopy (SEM). All the samples (MST-1, MST-2 and MST-3) exhibit nearly spherical images with uniform size distribution. The SEM studies evidently illustrate that the polysaccharide did not play a substantial part for producing the various morphologies of cobalt ferrite magnetic nanoparticles.

The transmission electron microscopic (TEM) studies have also been carried out to evaluate the effect of polysaccharides on the grain size, morphology and size distribution. Fig. 5 displays the TEM images of MST-1, MST-2 and MST-3 cobalt ferrite magnetic nanoparticles, which shows the formation of nearly regular and cuboidal shaped nanostructures. There is almost no effect of polysaccharides on the morphology but smallest size of 20 nm with cellulose and large size of 30 nm without polysaccharide was observed. The grain size of cobalt ferrite magnetic nanoparticles obtained from TEM studies was in close agreement with the X-ray size obtained from the Scherer's equation using X-ray line broadening studies (Table 1). The HRTEM studies have also been carried out for the structural analysis of cobalt ferrites. HRTEM image (Fig. 5) of sample MST-2 shows the well-defined lattice fringes which suggest the highly crystalline nature of the particles. The spacing of the two neighboring plane is about 0.262 nm, which is consistent with the inter–planar separation of the (3 1 1) plane in cubic (fcc) $CoFe_2O_4$.

Optical properties

The amount of light absorbed by any photocatalyst depends on their optical band gap energy (difference between valence band and conduction band). The optical band gap energy of cobalt ferrite

magnetic nanoparticles is shown in Fig. 6. It is well known that the optical band gap (Eg) can be calculated by the following equation:

$$(Ah\nu)^n = B(h\nu - Eg)$$

where $h\nu$ is the photon energy; *A* is absorbance, *B* is a constant related to the material; and *n* indicates either 2 or ½ for direct transition and indirect transition, respectively [40]. Hence, the optical band gap for the absorption peak can be obtained by extrapolating the linear portion of the $(Ah\nu)^n - h\nu$ curve to zero [41,42] as shown in insets of Fig. 6. The band gap values of synthesized materials are
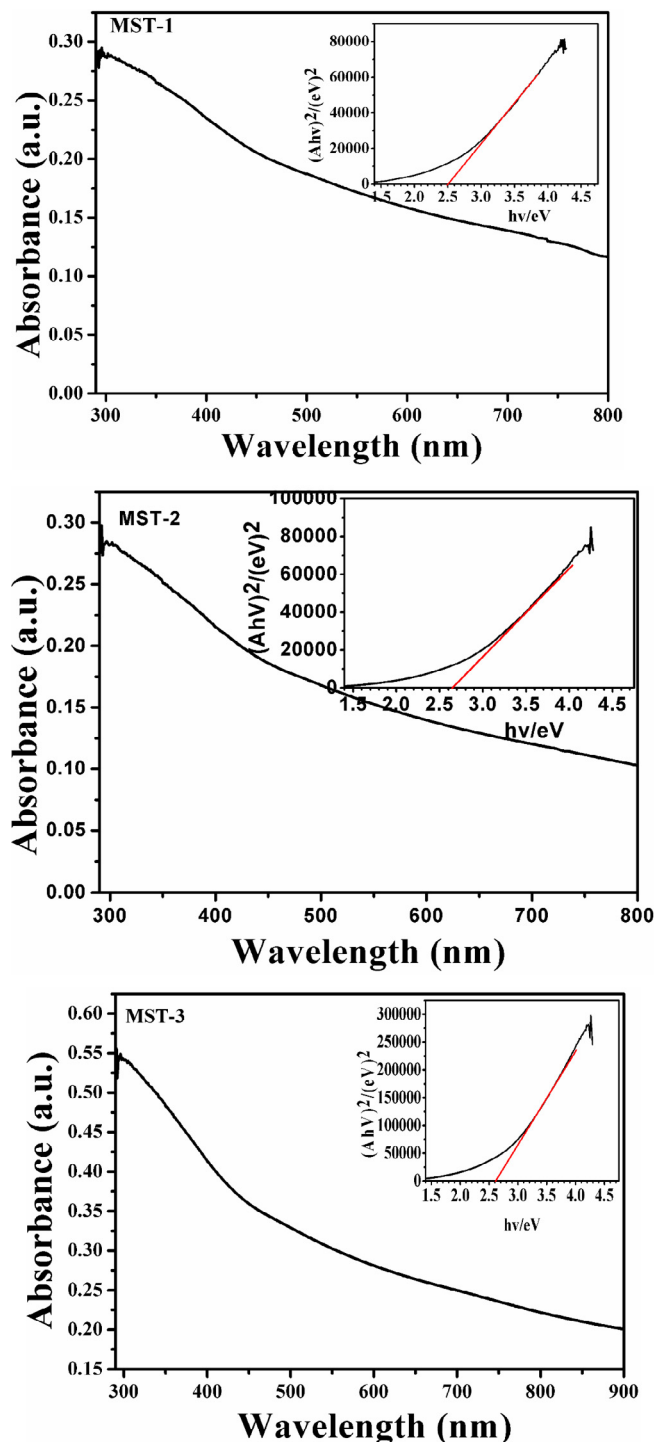

Fig. 6. UV–vis absorption spectrum and plots of $(Ah\nu)^n$ as a function of photon energy ($h\nu$) for the samples (MST-1, MST-2 and MST-3) nanoparticles.

summarized in Table 1, which corresponds to the visible-light photo activity. The energy band gap values obtained from present study is more similar to the reported in the literature [28].

Surface area properties

It is known that photocatalysis or catalysis skills depend on the size and surface area of photocatalysts. Fig. 7 represent the (a) BET plots (b) BJH pore size distribution (c) DH pore size distribution and (d) DA plots of cobalt ferrite ($CoFe_2O_4$) nanocomposites. The specific surface area, C constant, BJH pore radius, pore volume, DH pore radius, DA pore radius and micro pore volume of all cobalt ferrite magnetic nanoparticles calcined at 400 °C was measured and the values have been listed in Table 2. Among all prepared cobalt ferrite magnetic nanoparticles, the surface area of MST-2 is maximum at 76.0 m^2g^{-1} whereas for MST-1 its minimum occurs at 63.0 m^2g^{-1}, which is higher than $CoFe_2O_4$ prepared by the co-precipitation and other methods [43,44].

Photocatalytic activity of cobalt ferrite nanoparticles

Fig. 8 represented the UV–visible spectra of MB dye under visible light against the irradiation time by using three different photocatalysts and H_2O_2. UV–visible spectrophotometer was used to analyse the change in absorbance of MB dye at different time interval. A gradual change in colour of MB solution was observed with respect to time from blue to light blue and finally twisted to colourless which may be due to estrangement of the chromophoric

Table 2
BET surface area and pore parameters of (a) MST-1 (b) MST-2 (c) MST-3 Nanoparticles.

Sample		MST-1	MST-2	MST-3
BET	Surface area [$m^2 g^{-1}$]	63.00	76.00	64.00
	C constant	64.88	175.52	86.15
BJH	Pore radius [A°]	27.11	27.27	27.02
	Pore volume [$cm^3 g^{-1}$]	0.12	0.12	0.13
DH	Pore radius [A°]	27.11	27.27	27.02
	Pore volume [$cm^3 g^{-1}$]	0.12	0.12	0.13
DA	Pore radius [A°]	11.2	11.09	11.17
	Micropore volume [$cm^3 g^{-1}$]	0.078	0.075	0.078

group. The degradation of MB dye becomes faster rate due to two reasons:

(i) The photo decomposition of H_2O_2 results in the formation of hydroxyl radical (HO.) either by the electron–hole pair formation (e−/h+) on the surface of the cobalt ferrite magnetic nanoparticles, or by the electrons formed in the reaction mixture that are stuck directly by Fe^{3+} which can themselves react with H_2O_2 to form Fe^{2+}, which in turn can react with H_2O_2 to produce hydroxyl radicals.

(ii) High surface area, small size and reduced electron–hole recombination through electronic interaction in cobalt ferrite magnetic nanoparticles.
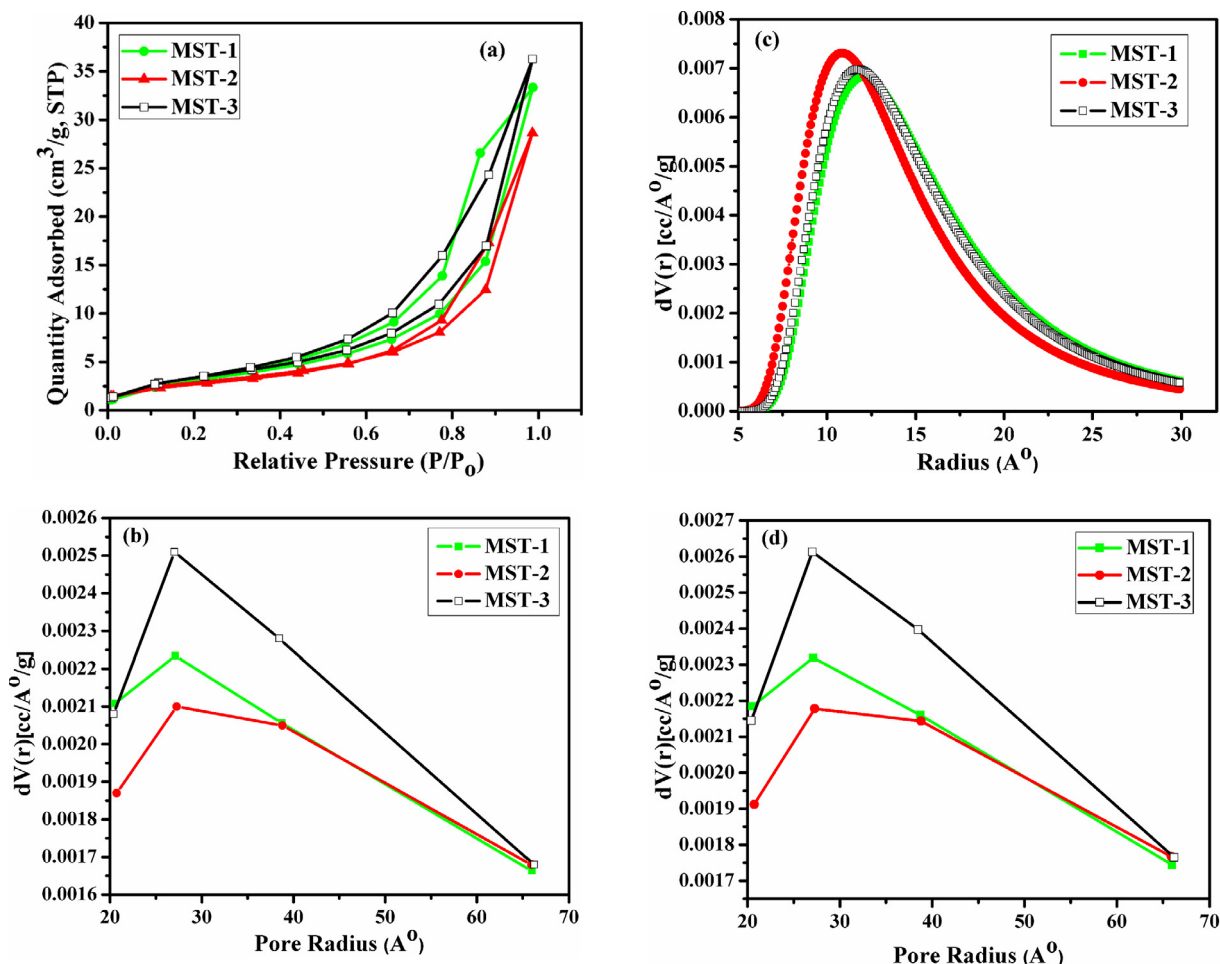

Fig. 7. (a) BET plots (b) BJH pore size distribution (c) DH pore size distribution and (d) DA plots of cobalt ferrite ($CoFe_2O_4$) nanoparticles.
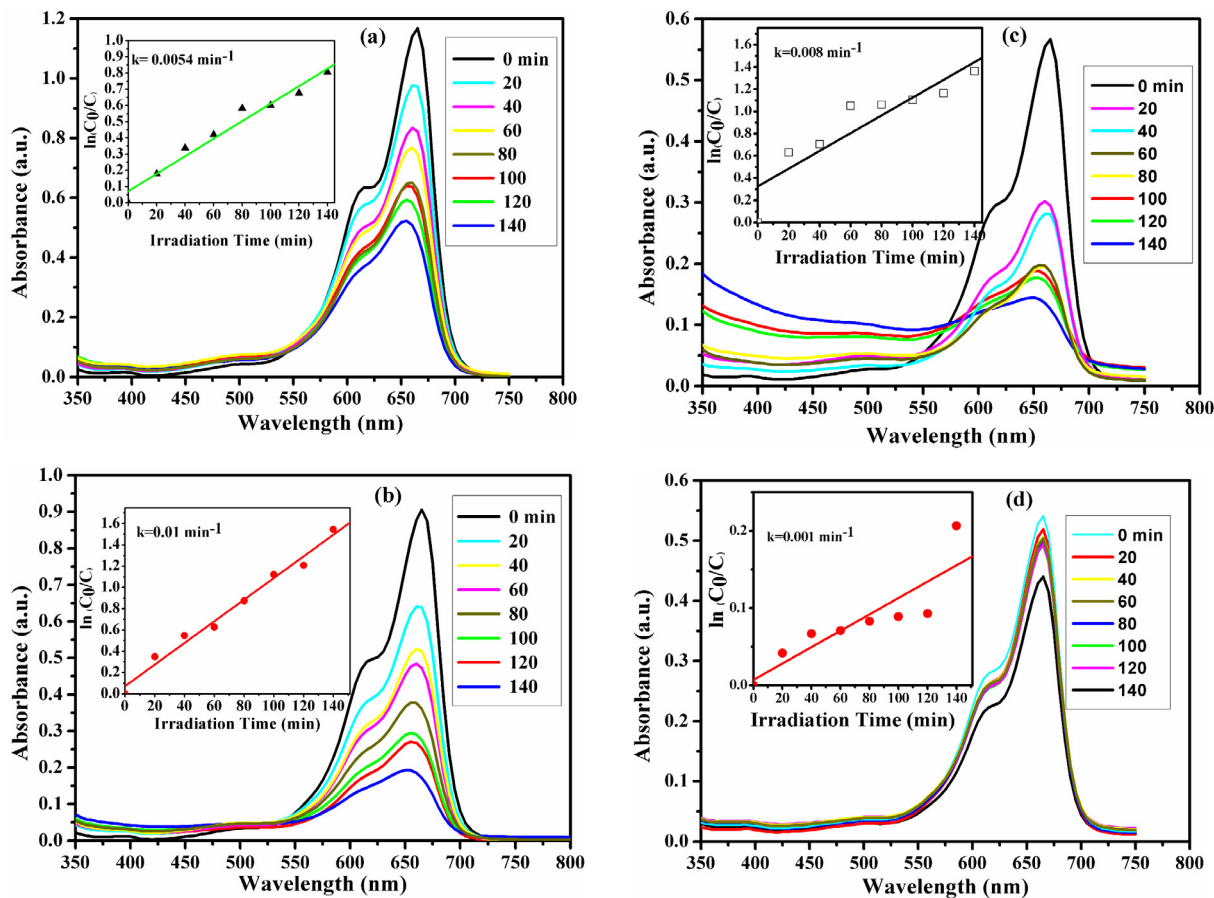
Fig. 8. UV–visible spectra of MB dye degraded by (a) MST-1, (b) MST-2 and (c) MST-3 nanoparticles. Inset represent plots of ln (C_0/C_t) Vs reaction time (min.) by (a) MST-1, (b) MST-2 and (c) MST-3 nanoparticles.

It is observed from the results that the photocatalytic efficiency maximum with MST-2 and minimum with MST-1 after 140 min irradiation. This may be due to effective separation, inhibition of electron-hole pair recombination and sufficient number of hydroxyl (·OH) radicals [45,46]. The order of efficiency of photocatalyst is MST-2 > MST-3 > MST-1.

It was also observed that the degradation rate of MB dye with MST-2 is very low in absence of H_2O_2 [Fig. 8d]. Many researchers have been reported such type of work but MST-2 shows improved photocatalytic activity [47,48]. It is well known that the materials having large band gap reduced the photo induced electron-hole pair and provide more place for charge carriers to go through active oxidation of MB dye. In addition, materials with small size show high surface area which provide more surfaces for dye to adsorb on the surface would go through surface reaction with hydroxyl (OH) radical formed on the catalyst surface.

Fig. 8a–d inset represent the photocatalytic degradation kinetics plots of MB dye using photocatalyst (MST-1, MST-2, MST-3) and H_2O_2 were assessed by using the first order rate equation:

$$\ln(C_0/C_t) = k1t$$

where C_0 is the initial concentration of MB dye solution, C_t is the concentration of MB solution at time t, k_1 is the first order rate constant, t is the visible light exposure time. The regression correlation coefficient (R^2) factor of the kinetics plots was used to obtained rate constant. The k_1 for MST-2 is 1.0×10^{-2} min^{-1} and is around 2.0 times faster than MST-1. In addition for MST-3 is also somewhat bigger than MST-1. This falling of rate constant is due to presence

of the fast recombination of electron- hole pairs that distresses the photocatalytic degradation process.

Conclusion

Nearly regular and cuboidal spinel structures (20–30.0 nm) of cobalt ferrite magnetic nanoparticles have been synthesized through modified solvothermal method at 400 °C. XRD results show the high purity of cobalt ferrite magnetic nanoparticles. The grain size of cobalt ferrite magnetic nanoparticles is in close agreement with the TEM and XRD studies. UV–visible studies show the optical band gaps of 2.50, 2.65 and 2.60 eV, which indicates cobalt ferrite magnetic nanoparticles may have visible-light photo catalytic activity. Among all, only MST-2 showed 80% degradation of MB dye within 140 min which was mainly due to the transfer of electron and hole to the surface of nanoparticles, hinder the electron hole recombination and high specific surface area. On the basis of the results, we can conclude that MST-2 nanoparticle would be beneficial for waste water treatment.

Acknowledgments

Appendix A. Supplementary data

Supplementary data associated with this article can be found, in the online version, at https://doi.org/10.1016/j.rinp.2018.01.045.

References

[1] Liu L, Zhang G, Wang L, Huang T, Qin L. Highly active S-modified $ZnFe_2O_4$ heterogeneous catalyst and its photo Fenton behavior under UVA visible irradiation. Ind Eng Chem Res 2011;50:7219.

[2] Bauer R, Waldner G, Fallmann H, Hager S, Klare M, Krutzler T, Malato S, Maletzky P. The photo-Fenton reaction and the TiO_2/UV process for waste water treatment novel developments. Catal Today 1999;53:131.

[3] Houas A, Lachheb H, Ksibi M, Elaloui E, Chantal G, Herrmann J-M. Photocatalytic degradation pathway of methylene blue in water. Appl Catal B Environ 2001;31:145.

[4] Ramirez JH, Vicente MA, Madeira LM. Heterogeneous photo-Fenton oxidation with pillared clay based catalysts for waste water treatment: a review. Appl Catal B Environ 2010;98:10.

[5] Gajovic A, Silva AMT, Segundo RA, Sturm S, Jancar B, Ceh M. Tailoring the phase composition and morphology of Bi-doped goethite-hematite nanostructure and their catalytic activity in the degradation of an actual pesticide using a photo-Fenton like process. Appl Catal B: Environ 2011;103:351.

[6] Wang Y, Zhao H, Li M, Fan J, Zhao G. Magnetic ordered mesoporous copper ferrite as a heterogeneous Fenton catalyst for the degradation of imidaclopride. Appl Catal B: Environ 2014;147:534.

[7] Fallmann H, Krutzler T, Bauer R, Malato S, Blanco J. Applicability of the photo-Fenton method for treating water containing pesticides. Catal Today 1999;54:309.

[8] Andreozzi R, Caprio V, Insola A, Marotta R. Advanced oxidation processes (AOP) for water purification and recovery. Catal Today 1999;53:51.

[9] Ghaly MY, Ha G, Mayer R, Haseneder R. Photochemical oxidation of p-chlorophenol by UV/H_2O_2 and photo-Fenton process. A comparative study. Waste Manage 2001;21:41.

[10] Liu SQ, Xiao B, Feng LR, Zhou SS, Chen ZG, Liu CB, Chen F, Wu ZY, Xu N, Oh WC, Meng ZD. Graphene oxide enhances the Fenton like photocatalytic activity of nickel ferrite for degradation of dyes under visible light irradiation. Carbon 2013;64:197.

[11] Garrido-Ramirez EG, Theng BKG, Mora ML. Clays and oxide minerals as catalysts and nanocatalysts in Fenton-like reactions- a review. Appl Clay Sci 2010;47:182.

[12] Maaz K, Mumtaz A, Hasanain SK, Ceylan A. Synthesis and magnetic properties of cobalt ferrite ($CoFe_2O_4$) nanoparticles prepared by wet chemical route. J Magn Magn Mater 2007;308:289.

[13] Sun Y, Wang W, Zhang L, Sun S, Gao E. Magnetic $ZnFe_2O_4$ octahedra: synthesis and visible light induced photocatalytic activities. Mater Lett 2013;98:124.

[14] Li HS, Zhang YP, Wang SY, Wu Q, Liu CH. Study on nanomagnets supported TiO_2 photocatalysts prepared by a sol–gel process in reverse microemulsion combining with solventthermal technique. J Hazard Mater 2009;169:1045.

[15] Yu L, Peng X, Ni F, Li J, Wang D, Luan Z. Arsenite removal from aqueous solutions by γ-Fe_2O_3-TiO_2 magnetic nanoparticles through simultaneous photocatalytic oxidation and adsorption. J Hazard Mater 2013;246:10.

[16] Xin T, Ma M, Zhang H, Gu J, Wang S, Liu M, Zhang Q. A facile approach for the synthesis of magnetic separable Fe_3O_4@TiO_2, core–shell nanocomposites as highly recyclable photocatalysts. Appl Surf Sci 2014;288:51.

[17] Zafar Q, Azmer MI, Al-Sehemi AG, Al-Assiri MS, Kalam A, Sulaiman K. Evaluation of humidity sensing properties of TMBHPETthin film embedded with spinel cobalt ferrite nanoparticles. J Nanopart Res 2016;18:186.

[18] Paulsen JA, Ring AP, Lo CCH, Snyder JE, Jiles DC. Manganese substituted cobalt ferrite magnetostrictive materials for magnetic stress sensor applications. J Appl Phys 2005;97:044502.

[19] Habibi MH, Parhizkar J. Cobalt ferrite nano-composite coated on glass by Doctor Blade method for photo-catalytic degradation of an azo textile dye Reactive Red 4: XRD, FESEM and DRS investigations. Spectrochim Acta Part A 2015;150:879.

[20] Alshehri SM, Alhabarah AN, Ahmed J, Naushad M, Ahmad T. An efficient and cost-effectivw tri-functional electrocatalyst based on cobalt ferrite embedded nitrogen doped carbon. J Colloid Interface Sci 2018;514:1.

[21] Pileni MP. Magnetic fluids: Fabrication, magnetic properties and organization of nanocrystals. Adv Funct Mater 2001;11:323.

[22] Kim DH, Nikles DE, Jhonson DT, Brazel CS. Heat generation of aqueously dispersed $CoFe_2O_4$ nanoparticles as heating agents for magnetically activated drug delivery and hyperthermia. J Magn Magn Mater 2008;320:2390.

[23] Erdem D, Bingham NS, Heiligtag FJ, Pilet N, Warnicke P, Heyderman LJ, Niederberger M. $CoFe_2O_4$ and $CoFe_2O_4$-SiO_2 nanoparticle thin films with perpendicular magnetic anisotropy for magnetic and magneto-optical applications. Adv Funct Mater 2016;26:1954.

[24] Ahmed J, Alshehri SM, Alhabarah AN, Ahmad T, Ahmad T. Nitrogen doped cobalt ferrite/carbon (NCFC) nanocomposites for supercapacitor application. Chem Electro Chem 2017;4:2952.

[25] Samavati A, Ismail AF. Antibacterial properties of copper-substituted cobalt ferrite nanoparticles synthesized by co-precipitation method. Particuology 2017;30:158.

[26] Casbeer E, Sharma VK, Li X-Z. Synthesis and photocatalytic activity of ferrites under visible light: a review. Sep Purif Technol 2012;87:1.

[27] Al-Shihri AS, Kalam A, Al-Sehemi AG, Du G, Ahmad T. One pot synthesis of Cobalt Ferrites nanoparticles via hydrothermal method and their optical studies. J Indian Chem Soc 2014;91:1861.

[28] Kiran VS, Sumathi S. Comparison of catalytic activity of bismuth substituted cobalt ferrite nanoparticles synthesized by combustion and co-precipitation method. J Magn Magn Mater 2017;421:113.

[29] Mattei YC, Pérez OP, Uwakweh ONC. Effect of high-energy ball milling time on structural and magnetic properties of nanocrystalline cobalt ferrite powders. J Magn Magn Mater 2013;341:17.

[30] Malik H, Mahmood A, Mahmood K, Lodhi MY, Warsi MF, Shakir I, Wahab H, Asghar M, Khan MA. Influence of cobalt substitution on the magnetic properties of zinc nanocrystals synthesized via micro-emulsion route. Ceram Int 2014;40:9439.

[31] Meron T, Rosenberg Y, Lereah Y, Markovich G. Synthesis and assembly of high-quality cobalt ferrite nanocrystals prepared by a modified sol–gel technique. J Magn Magn Mater 2005;292:11.

[32] Li S, Wang X. Synthesis of different morphologies lanthanum ferrite ($LaFeO_3$) fibers via electrospinning. Optik 2015;126:408.

[33] Raut AV, Barkule RS, Shengule DR, Jadhav KMJ. Synthesis, structural investigation and magnetic properties of Zn^{2+} substituted cobalt ferrite nanoparticles prepared by the sol–gel auto-combustion technique. J Magn Magn Mater 2014;358:87.

[34] Jiang J, Ai LH. Synthesis and characterization of Fe-Co binary ferrospinels nanospheres via one-step nonaqueous solution pathway. Mater Lett 2010;64:945.

[35] George M, Nair SS, John AM, Joy PA, Anantharaman MR. Structural, magnetic and electrical properties of the sol–gel prepared $Li_{0.5}Fe_{2.5}O_4$ fine particles. J Phys D: Appl Phys 2006;39:900..

[36] Duong GV, Turtelli RS, Hanh N, Linh DV, Reissner M, Michor H, Fidler J, Wiesinger G, Grössinger R. Magnetic properties of nanocrystalline $Co_{1-x}Zn_xFe_2O_4$ prepared by forced hydrolysis method. J Magn Magn Mater 2006;307:313.

[37] Li W, Li F-S. Structural and magnetic properties of $Co_{1-x}Zn_xFe_2O_4$ nanoparticles. Chin Phys B 2008;17:1858.

[38] Rani R, Sharma SK, Pirota KR, Knobel M, Thakur S, Singh M. Effect of zinc concentration on the magnetic properties of cobalt–zinc nanoferrite. Ceram Int 2012;38:2389.

[39] Ramalho MAF, Gama L, Antonio SG, Paiva-Santos CO, Miola EJ, Kiminami RHGA, Costa ACFM. X-Ray diffraction and mössbauer spectra of nickel ferrite prepared by combustion reaction. J Mater Sci 2007;42:3603.

[40] Hagfeldt A, Gratzel M. Light-induced redox reactions in nanocrystalline systems. Chem Rev 1995;95:49.

[41] Glasscock JA, Barnes PRF, Plumb IC, Bendavid A, Martin PJ. Structural, optical and electrical properties of undoped polycrystalline hematite thin film produced using filtered arc deposition. Thin Solid Films 2008;516:1716.

[42] Liu B, Wen L, Zhao X. The structure and photocatalytic studies of N-doped TiO_2 films prepared by radio frequency reactive magnetron sputtering. Sol Energy Mater Sol Cells 2008;92:1.

[43] Jiao Z, Geng X, Wu M, Jiang Y, Zhao B. Preparation of $CoFe_2O_4$ nanoparticles by spraying co-precipitation and structure characterization. Colloids Surf A 2008;313:31.

[44] Jauhar S, Singhal S, Dhiman M. Manganese substituted cobalt ferrites as efficient catalysts for H_2O_2 assisted degradation of cationic and anionic dyes: their synthesis and characterization. Appl Catal A 2014;486:210.

[45] Roy TK, Mondal NK. Photocatalytic degradation of congo red dye on thermally activated zinc oxide. Int J Sci Res Environ Sci 2014;2:457.

[46] Han L, Zhou X, Wan L, Deng Y. Synthesis of $ZnFe_2O_4$ nanoplates by succinic acid- assisted hydrothermal route and their photocatalytic degradation of rhodamine B under visible light. J Environ Chem Eng 2014;2:123.

[47] Talukdar S, Mandal D, Mandal K. Surface modification of Cobalt ferrite nano-hollow spheres for inherent multiple photoluminescence and enhanced photocatalytic activities. Chem Phys Lett 2017;672:57.

[48] Wu X, Wang W, Li F, Khaimanov S, Tsidaeva N, Lahoubi M. PEG-assisted hydrothermal synthesis of $CoFe_2O_4$ nanoparticles with enhanced selective adsorption properties for different dyes. Appl Sur Sci 2016;389:1003.